Computational Modeling of Electro-Elasto-Capillary Phenomena in Dielectric Elastomers

Saman Seifi[a], Harold S. Park[b]

[a]*Department of Mechanical Engineering, Boston University, Boston, MA 02215*
[b]*Department of Mechanical Engineering, Boston University, Boston, MA 02215*

Abstract

We present a new finite deformation, dynamic finite element model of dielectric elastomers that incorporates surface tension to capture elastocapillary effects on the electromechanical deformation.

Keywords: dielectric elastomer, elastocapillary

1. Introduction

Dielectric elastomers (DEs) have attracted significant attention in recent years as a soft and flexible actuation material (Carpi et al., 2010; Brochu and Pei, 2010; Biddiss and Chau, 2008). The salient characteristic of DEs is that if sandwiched between two compliant electrodes that apply voltage across its thickness, the DE can exhibit both significant thinning and in-plane expansion, where the in-plane expansion can often exceed several hundred percent (Keplinger et al., 2012). The ability to undergo such large deformations has led to DEs being studied for both actuation-based applications, including artificial muscles and flexible electronics, and also for generation-based applications and energy harvesting (Carpi et al., 2010; Brochu and Pei, 2010; Mirfakhrai et al., 2007).

Detailed studies on the mechanics of DEs began about 15 years ago with the seminal experimental work of Pelrine et al. (1998, 2000). Since then, there have been many experimental (Fox and Goulbourne, 2008; Keplinger et al., 2010; Kofod et al., 2003; Kofod and Sommer-Larsen, 2005; Pei et al., 2004; Plante and Dubowsky, 2006, 2007a,b;

Schlaak et al., 2005; Wissler and Mazza, 2007; Zhang et al., 2004; Chiba et al., 2008; Wang et al., 2011b, 2012b,a), theoretical (Suo et al., 2008; Suo, 2010; Goulbourne et al., 2005; Dorfmann and Ogden, 2005, 2006; McMeeking and Landis, 2005; Patrick et al., 2007; Plante and Dubowsky, 2007a,b; Wissler and Mazza, 2005), and recently a small number of computational studies (Park et al., 2012; Park and Nguyen, 2013; Park et al., 2013; Zhou et al., 2008; Zhao and Suo, 2007; Vu et al., 2007; Wissler and Mazza, 2005; Buschel et al., 2013; Khan et al., 2013; Henann et al., 2013; Li and Landis, 2012) aimed that identifying the mechanisms that have the largest impact on the nonlinear dynamical behavior and failure mechanisms of DEs. A summary of recent developments on electromechanical instabilities in DEs has been given by Zhao and Wang (2014).

Concurrently, researchers have for many years studied the forces exerted by fluids at rest upon solids, which are known as surface tension, or elastocapillary forces. While the best-known example of surface tension is likely that of deforming liquid droplets, there has been interest in using it to deform solid structures, see the reviews of Roman and Bico (2010) and Liu and Feng (2012). Specifically, there has recently been interest in using elastocapillary forces to deform *soft* structures in controllable or unique ways, since for these systems the elastocapillary number, which is defined as $\gamma/\mu l$, where γ is the surface tension, μ is the shear modulus and l is a characteristic length, is close to unity, implying that elastocapillary effects can be substantial

URL: `samansei@bu.edu` (Saman Seifi), `parkhs@bu.edu` (Harold S. Park)

[0a]*Department of Mechanical Engineering, Boston University, Boston, MA 02215, USA. E-mail: samansei@bu.edu*

[0*b]*Department of Mechanical Engineering, Boston University, Boston, MA 02215, USA. Fax: 001 617 353 5866; Tel: 001 617 353 4208; E-mail: parkhs@bu.edu*

for these soft materials.

While elastocapillary effects have been extensively studied in soft materials, its effect on soft materials like DEs that deform when subject to an electric field, is a relatively unknown phenomenon. For example, Wang and Zhao (2013) performed interesting experiments of electrostatically deforming a constrained DE in a liquid solution, and showed that the instability mechanism of the surface could be tuned depending on the value of the surface tension. Furthermore, Pineirua et al. (2010) showed how elastocapillary origami could be developed by coupling surface tension with electric fields to deform a liquid droplet surrounded by a thin sheet of PDMS. Overall, this discussion makes clear that there may be potential in using surface tension as an additional degree of freedom to introduce new and interesting deformation mechanisms in electroactive polymers like DEs, and furthermore that the computational tools needed to investigate such phenomena are currently lacking.

Therefore, the objective of the present work is to present a finite element (FE) model for DEs accounting for the effects of surface tension, such that electro-elasto-capillary phenomena in DEs can be computationally investigated. We pay particular interest to those instances where surface tension couples to and impacts known electromechanical instabilities that dielectric elastomers are known to undergo, specifically snap-through instability (Pelrine et al., 2000) and surface creasing and wrinkling (Wang et al., 2011a, 2012b; Wang and Zhao, 2013). ion as an additional degree of freedom to introduce new and interesting deformation mechanisms in electroactive polymers like DEs, and furthermore that the computational tools needed to investigate such phenomena are currently lacking.

Therefore, the objective of the present work is to present a finite element model for DEs accounting for the effects of surface tension, such that electro-elasto-capillary phenomena in DEs can be computationally investigated. We pay particular interest to those instances where surface tension couples to and impacts known electromechanical instabilities that dielectric elastomers are known to undergo, specifically snap-through instability (Pelrine et al., 2000), surface creasing (Wang et al., 2011a, 2012b), and bursting drops leading to crack-like propagation (Wang et al., 2012a).

2. Background: Nonlinear Electromechanical Field Theory

The numerical results we present in this work are based upon a finite element (FEM) discretization of the electromechanical field theory recently proposed by Suo et al. (2008), and recently reviewed by Suo (2010). In this field theory at mechanical equilibrium, the nominal stress S_{iJ} satisfies the following (weak) equation:

$$\int_V S_{iJ} \frac{\partial \xi_i}{\partial X_J} dV = \int_V \left(B_i - \rho \frac{\partial^2 x_i}{\partial t^2} \right) \xi_i dV + \int_A T_i \xi_i dA, (1)$$

where ξ_i is an arbitrary vector test function, B_i is the body force per unit reference volume V, ρ is the mass density of the material and T_i is the force per unit area that is applied on the surface A in the reference configuration.

For the electrostatic problem, the nominal electric displacement $\tilde{D}_I$ satisfies the following (weak) equation:

$$-\int_V \tilde{D}_I \frac{\partial \eta}{\partial X_I} dV = \int_V q\eta dV + \int_A \omega\eta dA, \quad (2)$$

where η is an arbitrary scalar test function, q is the volumetric charge density and ω is the surface charge density, both with respect to the reference configuration. It can be seen that the strong form of the mechanical weak form in (1) is the momentum equation, while the strong form of the electrostatic weak form in (2) is Gauss's law.

As the governing field equations in (1) and (2) are decoupled, the electromechanical coupling occurs through the material laws. The hyperelastic material law we adopt here has been utilized in the literature to study the nonlinear deformations of electrostatically actuated polymers; see the works of Vu et al. (2007), and Zhao and Suo (2007). Due to the fact that the DE is a rubber-like polymer, phenomenological free energy expressions are typically used to model the deformation of the polymer chains. In the present work, we will utilize the form (Vu et al., 2007; Zhao and Suo, 2007)

$$W(\mathbf{C}, \tilde{\mathbf{E}}) = \mu W_0 - \frac{1}{2}\lambda(\ln J)^2 - 2\mu W_0(3)\ln J - \frac{\epsilon}{2}JC_{IJ}^{-1}\tilde{E}_I\tilde{E}_J, (3)$$

where W_0 is the mechanical free energy density in the absence of an electric field, ϵ is the permittivity, $J = \det(\mathbf{F})$, where $\mathbf{F}$ is the continuum deformation gradient, C_{IJ}^{-1} are the components of the inverse of the right Cauchy-Green tensor $\mathbf{C}$, λ is the bulk modulus and μ is the shear modulus.

We model the mechanical behavior of the DE using the Arruda-Boyce rubber hyperelastic function (Arruda and Boyce, 1993), where the mechanical free energy W_0 in (3) is approximated by the following truncated series expansion,

$$W_0(I_1) = \frac{1}{2}(I_1 - 3) + \frac{1}{20N}(I_1^2 - 9) + \frac{11}{1050N^2}(I_1^3 - 27) \quad (4)$$
$$+ \frac{19}{7000N^3}(I_1^4 - 81) + \frac{519}{673750N^4}(I_1^5 - 243),$$

where N is a measure of the cross link density, I_1 is the trace of $\mathbf{C}$, and where the Arruda-Boyce model reduces to a Neo-Hookean model if $N \to \infty$. We note that previous experimental studies of Wissler and Mazza (2007) have validated the Arruda-Boyce model as being accurate for modeling the large deformation of DEs.

3. Finite Element Formulation

3.1. Nonlinear, Dynamic Finite Element Model

The FEM model we use was previously developed by Park et al. (2012). In that work, the corresponding author and collaborators developed a nonlinear, dynamic finite element (FEM) formulation of the governing nonlinear electromechanical field equations of Suo *et al.* Suo et al. (2008) that are summarized in (1) and (2). By using a standard Galerkin FEM approximation to both the mechanical displacement and electric potential fields, and incorporating inertial effects in the mechanical momentum equation, an implicit, coupled, monolithic nonlinear dynamic FEM formulation was obtained with the governing equations (Park et al., 2012)

$$\begin{pmatrix} \Delta \mathbf{a} \\ \Delta \mathbf{\Phi} \end{pmatrix} = - \begin{pmatrix} \mathbf{M} + \beta \Delta t^2 \mathbf{K}^{mm} & \mathbf{K}^{me} \\ \beta \Delta t^2 \mathbf{K}^{em} & \mathbf{K}^{ee} \end{pmatrix} \begin{pmatrix} \mathbf{R}^{mech} \\ \mathbf{R}^{elec} \end{pmatrix} \quad (5)$$

where $\Delta \mathbf{a}$ is the increment in mechanical acceleration, $\Delta \mathbf{\Phi}$ is the increment in electrostatic potential, $\beta = 0.25$ is the standard Newmark time integrator parameter, $\mathbf{R}^{mech}$ is the mechanical residual, $\mathbf{R}^{elec}$ is the electrical residual, and the various stiffness matrices $\mathbf{K}$ include the purely mechanical ($\mathbf{K}^{mm}$), mixed electromechanical ($\mathbf{K}^{me} = \mathbf{K}^{em}$), and purely electrostatic ($\mathbf{K}^{ee}$) contributions. Details regarding the residual vectors and the various mechanical, electromechanical and electrostatic stiffnesses can be found in previous work (Park et al., 2012).

In the present work, volumetric locking due to the incompressible material behavior was alleviated using the Q1P0 method of Simo et al. (1985). While
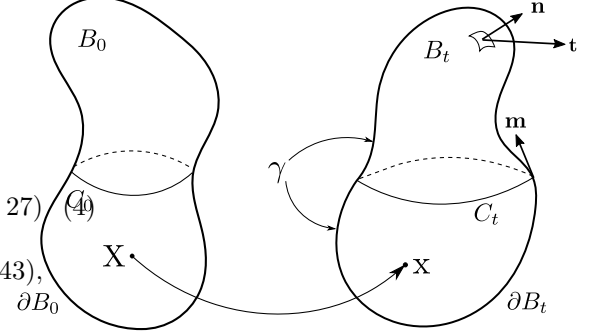

Figure 1: The reference body B_0 and the deformed body B_t at time t.

viscoelastic effects have previously been accounted for within the FEM model (Park and Nguyen, 2013), these effects are neglected in the present work such that the effects of surface tension on electromechanical instabilities in DEs can be investigated without other physical complications.

3.2. Surface Tension

Finite element formulations of surface tension have been given by Saksono and Peric (2006a) and Javili and Steinmann (2010), amongst others. We note that the recently published work of Henann and Bertoldi (2014) uses the model presented by Saksono and Peric (2006a), with an incompressible hyperelastic material model for the deforming solid. In the present work, we utilize the dynamic formulation of Saksono and Peric (2006b), where the utility and importance of using inertia to capture, using FEM, the electromechanical instabilities that occur in DEs was shown in the previous works of Park et al. (2012, 2013); Park and Nguyen (2013). We now briefly describe the formulation, and the resulting electro-elasto-capillary FEM equations that we solve, while a schematic of the current and reference configurations is shown in Figure (1).

Using the Saksono and Peric (2006b) model, we begin with the force continuity at the solid-liquid interface,

$$\sigma \mathbf{n} = -p_{ext}\mathbf{n} + 2H\gamma\mathbf{n} \quad (6)$$

where $\mathbf{n}$ is the unit normal, σ is the Cauchy stress, H is the mean curvature, and p_{ext} is an external pressure. The spatial (updated Lagrangian) form of the weak form of the momentum equation can

then be written as

$$\int(\sigma : \nabla \mathbf{w} - \rho(\mathbf{b} - \mathbf{a}) \cdot \mathbf{w})dv - \int \mathbf{t} \cdot \mathbf{w}da - \int(-p_{ext}\mathbf{n} \cdot \mathbf{w})da \quad (7)$$
$$+ \int(\gamma \nabla_s \cdot \mathbf{w})da - \int(\gamma \mathbf{w} \cdot \mathbf{m})ds = 0$$

where $\mathbf{w}$ is the virtual displacement, $\mathbf{t}$ is the traction, $\mathbf{b}$ is the body force, $\nabla_s = (\mathbf{I} - \mathbf{n} \otimes \mathbf{n})\nabla$ is the surface gradient operator, ρ is the density and $\mathbf{a}$ is the acceleration. In the present work, we neglect the three-phase contact line, i.e. the integral in (7) over the line ds for simplicity.

The FEM form of (7) can be obtained by making the usual Galerkin approximation of both the displacements and virtual displacements with the same shape functions, resulting in the (mechanical) residual $\mathbf{R}^{mech}(\mathbf{X})$

$$\mathbf{R}^{mech}(\mathbf{X}) = \mathbf{M}\ddot{\mathbf{X}} + \mathbf{F}^{int} - \mathbf{F}^{ext} + \mathbf{F}^{surf} = 0 \quad (8)$$

where the various terms in (8) take the following form for each FE e

$$\mathbf{M}_e = \int \rho \mathbf{N}^T \mathbf{N} dv \quad (9)$$

$$\mathbf{F}_e^{int} = \int \mathbf{B}^T \sigma dv$$

$$\mathbf{F}_e^{ext} = \int \mathbf{N}^T \mathbf{b} dv + \int \mathbf{N}^T \mathbf{t} da$$

$$\mathbf{F}_e^{surf} = \int \gamma \nabla_s \mathbf{N} da$$

where $\mathbf{N}$ and $\mathbf{B}$ are the standard FEM shape function and gradient, respectively. As can be seen in (8), the only non-standard term compared to the standard discretization of the momentum equation arises in the surface force $\mathbf{F}^{surf}$, and the corresponding surface stiffness $\mathbf{K}^{surf}$.

Henann and Bertoldi (2014) analytically derived the surface force $\mathbf{F}^{surf}$ for a two-dimensional, 4-node bilinear quadrilateral element as

$$\mathbf{F}^{surf} = -\frac{h\gamma}{L_e} \begin{pmatrix} x_1 - x_2 \\ y_1 - y_2 \\ x_2 - x_1 \\ y_2 - y_1 \end{pmatrix} \quad (10)$$

The surface stiffness $\mathbf{K}^{surf}$ can be obtained through linearization of the surface force $\mathbf{F}^{surf}$ in (8). This value for a 4-node bilinear quadrilateral element in two-dimensions was also given analytically
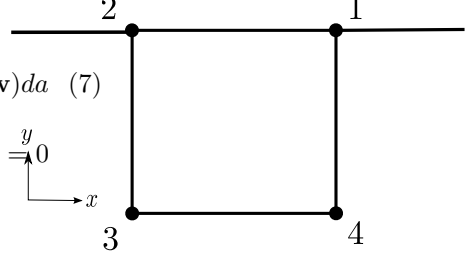

Figure 2: Schematic of nodal numbering consistent with surface tension formulation given in Eqs. (10) and (11). Nodes 1 and 2 are surface nodes.

by Henann and Bertoldi (2014) as

$$\mathbf{K}^{surf} = \frac{h\gamma}{L_e} \begin{pmatrix} 1 & 0 & -1 & 0 \\ 0 & 1 & 0 & -1 \\ -1 & 0 & 1 & 0 \\ 0 & -1 & 0 & 1 \end{pmatrix} - \frac{h\gamma}{L_e^3} \begin{pmatrix} x_1 - x_2 \\ y_1 - y_2 \\ x_2 - x_1 \\ y_2 - y_1 \end{pmatrix} \begin{pmatrix} a \\ y \\ a \\ y \end{pmatrix}$$

where L_e is the length of the FE face containing nodes 1 and 2. The ordering of the FE nodes corresponding to Eqs. (10) and (11) is shown in Fig. (2).

The final coupled electromechanical FEM equations we solve, which include the surface tension terms, can be written as

$$\begin{pmatrix} \Delta \mathbf{a} \\ \Delta \mathbf{\Phi} \end{pmatrix} = -\begin{pmatrix} \mathbf{M} + \beta \Delta t^2(\mathbf{K}^{mm} + \mathbf{K}^{surf}) & \mathbf{K}^{me} \\ \beta \Delta t^2 \mathbf{K}^{em} & \mathbf{K}^{ee} \end{pmatrix}\begin{pmatrix} \mathbf{R}^{me} \\ \mathbf{R}^{el} \end{pmatrix}$$

In comparing the new FE formulation including surface tension in (12) to the previous FEM equations of Park et al. (2012) in (5), the only changes are the addition of the surface stiffness $\mathbf{K}^{surf}$ to the standard mechanical stiffness matrix $\mathbf{K}^{mm}$, as well as the surface contribution $\mathbf{F}^{surf}$ to the mechanical residual $\mathbf{R}^{mech}$, as shown previously in (8) and (9).

4. Numerical Results

All numerical simulations were performed using the open source code Tahoe (2015) with standard 4-node, bilinear quadrilateral finite elements within a two-dimensional, plane strain approximation. Before any application of electrostatic loading via applied charges or voltages, the surface tension is first applied incrementally until the desired value is reached; the incremental approach is necessary to avoid computational instabilities, as previously discussed by Javili and Steinmann (2010). The surface tension is applied incrementally by defining a
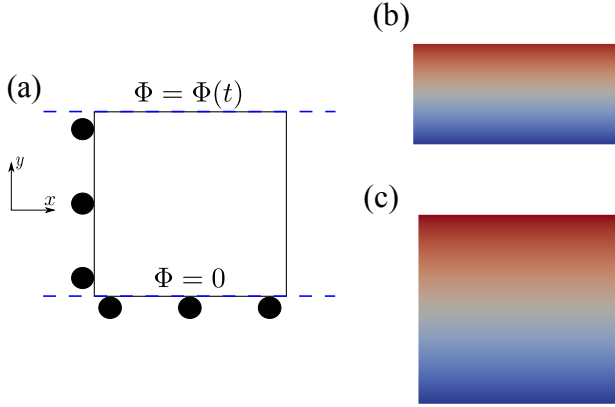
Figure 3: (a) Schematic of single element with homogeneous boundary conditions; (b) Deformed configuration with $\gamma = 0$; (c) Deformed configuration with $\gamma = 10$.

target value of surface tension γ we define the following function γ_0:

$$\gamma_0 = min\left(\gamma, \frac{\gamma t}{t_0}\right) \qquad (13)$$

where t is the current time and t_0 is the total time allotted to reach the prescribed value for surface tension γ. Once the system is in equilibrium with the surface tension, voltage or charge is applied in a monotonically increasing fashion.

4.1. Single Element Tests

We first perform a suite of parametric benchmark studies to gain a qualitative understanding of how surface tension impacts the electromechanical behavior of DEs undergoing homogeneous and inhomogeneous deformation. A single 4-node bilinear quadrilateral element of unit length and height is used for these simulations. For all numerical simulations, we chose the following constitutive parameters for the Arruda-Boyce model in Eq. (4): $\mu = \epsilon = 1$, $\lambda = 1000$ and $N = 5.0$, while different values of the surface tension γ are chosen.

4.1.1. Homogeneous Deformation

The first set of boundary conditions are to allow homogeneous deformation of the DE. The electromechanical boundary conditions are as shown in Fig. (3)(a), with rollers on the -x and -y surfaces, and voltage applied at the top surface of

the single square element. The resulting configurations for surface tension values of $\gamma = 0$ and $\gamma = 10$ are shown in Figures (3)(b) and (c). As can be seen, Figure (3)(b) shows the well-known deformed configuration where the DE contracts along the thickness direction while simultaneously elongating in response to the applied voltage. However, the configuration in Figure (3)(c) is quite different when $\gamma = 10$. Instead of resulting in a rectangular deformed configuration, the single element takes a deformed configuration that does not appear much changed from the initial, square configuration, which shows that the impact of surface tension is to resist the deformation that would otherwise occur due to the applied voltage.

We plot the resulting normalized voltage-charge curves in Figure (4) for various values of γ. We can see that the effect of increasing surface tension is to increase the voltage that is required to induce the electromechanical instability. These results are quantitatively in agreement with previous experimental and theoretical studies on soft materials which found that the effect of surface tension is to create a barrier to instability nucleation (Chen et al., 2012; Mora et al., 2011). We also note that a softening response is not observed in the voltage-charge plot due the fact that a plane strain, and not plane stress (Zhou et al., 2008) approximation in two dimensions is utilized. [*hsp*: What is the normalized value of voltage when $\gamma = 100$ for which the electromechanical instability occurs, i.e. how much is this critical voltage increased as compared to the $\gamma = 0$ case?]

4.1.2. Inhomogeneous Deformation

Before studying surface tension effects on inhomogeneously deforming DEs, as will be done in subsequent computational examples, we first study a single FE that is fully constrained mechanically along its bottom surface, as illustrated in Figure (5)(a). If no surface tension is present, i.e. $\gamma = 0$, the top surface of the element bows outward in response to the applied voltage. However, for non-zero surface tension $\gamma = 10$, the large outward bowing of the top surface that was observed for $\gamma = 0$ in Figure (5)(b) is reduced drastically, as shown in Figure (5)(c). The effect of the surface tension opposing the deformation that is induced by the voltage is similar to that previously observed for the homogeneous boundary conditions.

We also analyze the voltage-charge curve for different values of γ in Figure (6). As can be seen,
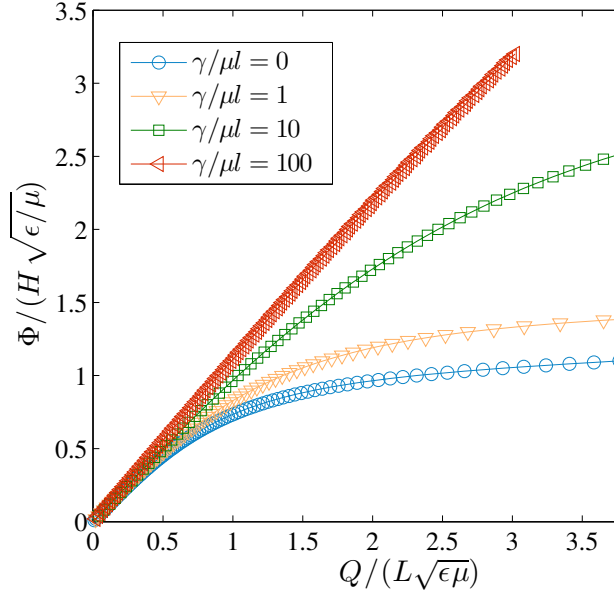
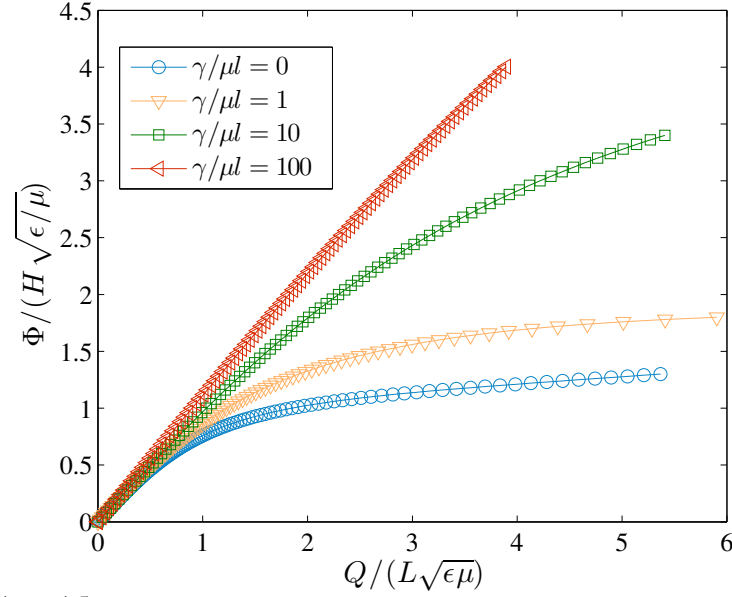Figure 4: Deformation of a single, homogeneously deforming FE subject to voltage loading.

Figure 6: Deformation of a single, inhomogeneously deforming FE subject to voltage loading.
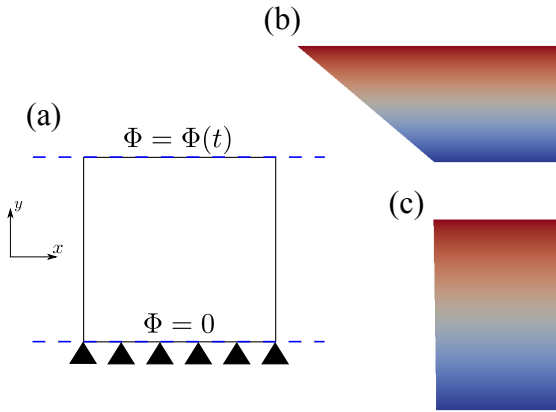

Figure 5: (a) Schematic of single element with inhomogeneous boundary conditions; (b) Deformed configuration with $\gamma = 0$; (c) Deformed configuration with $\gamma = 10$.

the major effect of surface tension is again to significantly increase the value of voltage Φ that is required in order to induce the voltage-induced electromechanical snap-through instability.

4.2. Surface Creasing in 2D Strip

Our next example is based on recent experiments by Wang and Zhao (2013), who studied the surface instability mechanisms in constrained DE films in which the top surface is immersed in a fluid. The fluid was varied such that the top surface of the DE film was subject to different values of surface tension. Interestingly, upon application of a critical voltage, a transition in the surface instability mechanism from creasing to wrinkling was observed, which was found to be dependent on elastocapillary length $\gamma/(\mu H)$. Along with the transition in surface instability mechanism, the wavelength of the instability was also found to change, from about $\lambda = 1.5H$ for the creasing instability to longer wavelengths, $\lambda = 5 - 12H$ when the elastocapillary length $\gamma/(\mu H) > 1$.

We performed FE simulations of the experiments of Wang and Zhao (2013), where the schematic of the problem geometry and the relevant electromechanical boundary conditions is shown in Figure (7), i.e. the left, right and bottom surfaces of the
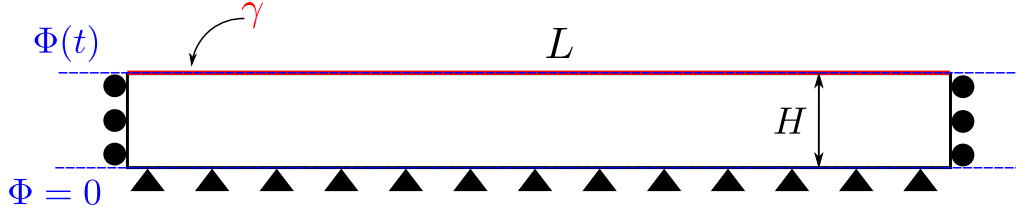
6

Figure 7: Schematic of the film with electro-elasto-capillary boundary conditions.

film are fixed while a voltage is applied to the top surface, where the surface tension is also present.

We show in Figure (8)(a) the difference in surface instability mechanism depending on the elastocapillary length. As can be seen, when the surface tension is small, or completely negligible, the surface instability mechanism is that of creasing, or localized folds. As the elastocapillary length increases to become similar to the film height, the surface instability mechanism changes to wrinkling, as shown in Figure (8)(b). The change in instability mechanism is characterized by a significantly larger instability wavelength as compared to the creasing instability in Figure (8)(a). Furthermore, rather than abrupt, localized folds as in the creasing instability in Figure (8)(a), the surface exhibits a more gradual undulating pattern as seen in Figure (8)(b).

This instability transition was also characterized experimentally by plotting the normalized electric field $E_c / \sqrt{\mu/\epsilon}$ and the normalized wavelength λ/H as a function of the elastocapillary length Wang and Zhao (2013), as shown in Figure (10). For elastocapillary numbers $\gamma/(\mu H) < 1$, we find the normalized wavelength λ/H to be close to the value of 1.5 predicted theoretically Wang and Zhao (2013). For larger elastocapillary numbers, i.e. $\gamma/(\mu H) > 1$, where wrinkling is observed, a dramatic increase in normalized instability wavelength λ/H is observed. [*hsp*: The slope of our curve in Figure 9 appears to be different than Figure 4b in the Wang and Zhao 2013 PRE paper, or is it? Our values for elastocapillary numbers larger than one are smaller than the theory. You should look through the theory to see if there's any 2D vs. 3D difference.] [*ss*: In their experiment $\gamma = 0.04 \ N/m$ but $\gamma/\mu H$ is the in the range we used]

[*hsp*: Need here: (1) Figure like FIgure 4(a) in the Wang and Zhao PRE paper for the critical electric field vs. elastocapillary length.]

(a) creasing $\dfrac{\gamma}{\mu H} = 0.5$

(b) wrinkling $\dfrac{\gamma}{\mu H} = 8$

Figure 8: Computationally observed transition in the surface instability mechanism in DEs as a function of the elastocapillary length $\gamma/(\mu H)$, for a DE film of dimensions 160x4. [*hsp*: In figure a, the displacement magnitude of 6.25 is larger than the film thickness of 4. That is obviously not physical.]
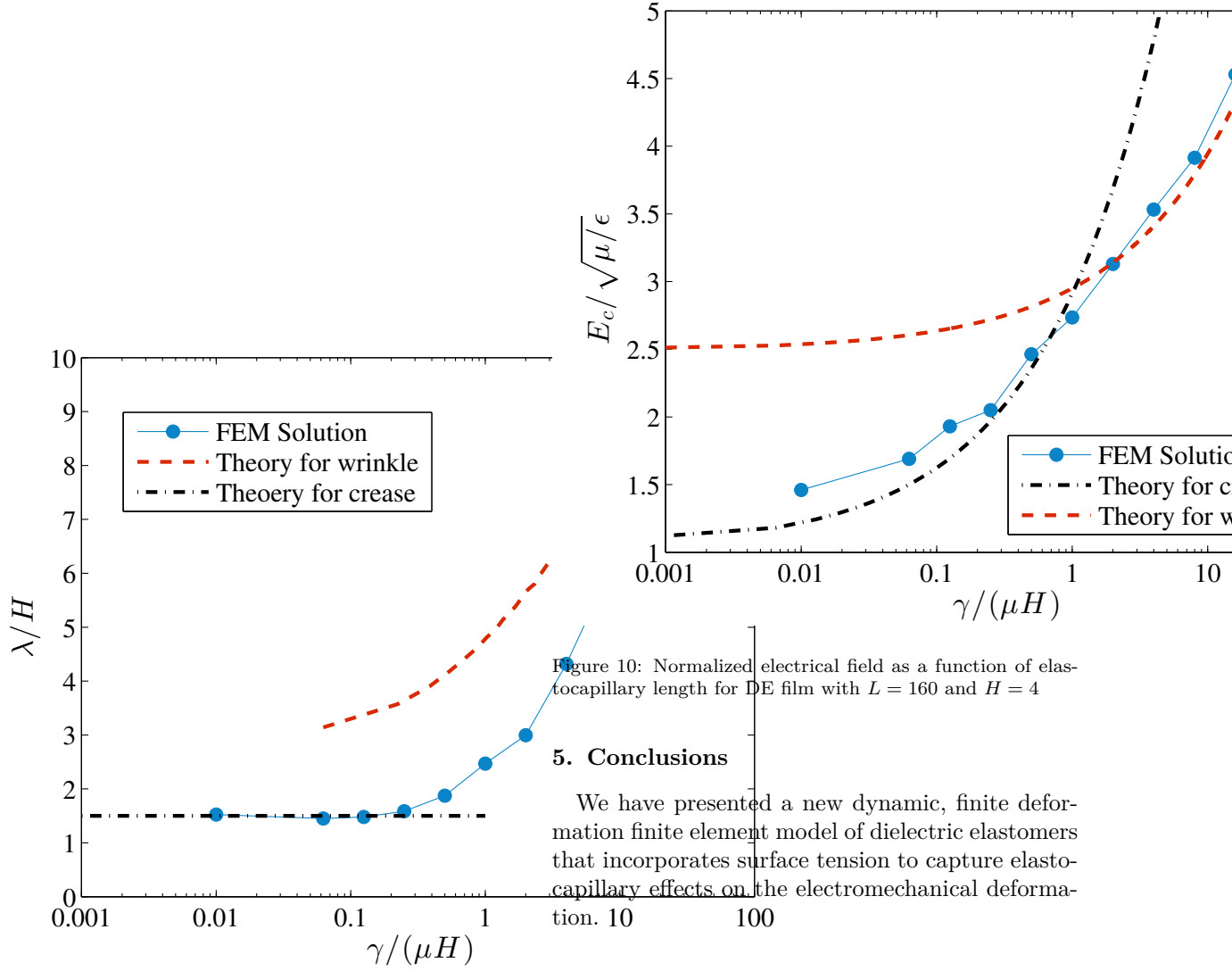
Figure 9: Normalized instability wavelength as a function of elastocapillary length for 160x4 DE film for two different mesh spacing e. [*ss*: The agreement with wrinkling theory and our results are not good!]

Figure 10: Normalized electrical field as a function of elastocapillary length for DE film with $L = 160$ and $H = 4$

5. Conclusions

We have presented a new dynamic, finite deformation finite element model of dielectric elastomers that incorporates surface tension to capture elastocapillary effects on the electromechanical deformation.

6. Acknowledgements

7. Appendix

We show here verification of the 2D Q1P0 formulation in alleviating volumetric locking. To do so, we compare it to results obtained using a single 8-node hexahedral element with the previously published Q1P0 formulation of Park et al. (2013). The 2D results were obtained using the 2D version of the Q1P0 formulation of Simo et al. (1985); the boundary conditions on the single 4-node quadrilateral 2D finite element were the same as those previously seen in Figure (5)(a). For the 3D element,
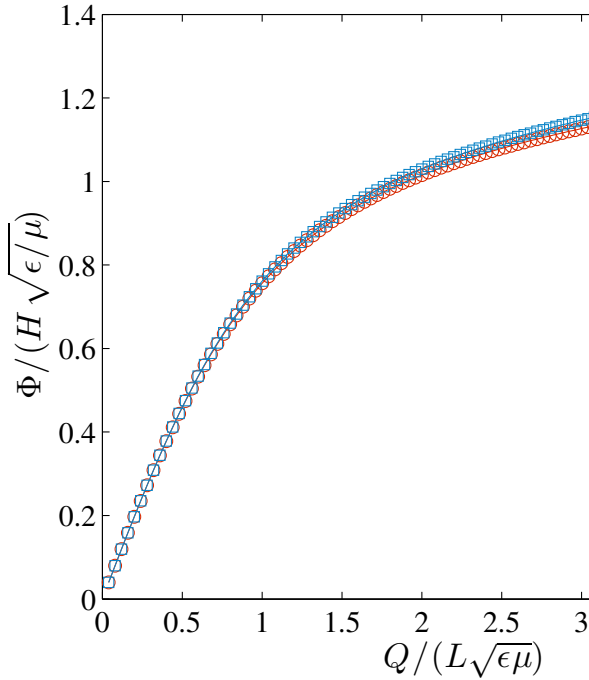
in addition to having its bottom surface completely constrained, all z-displacements were set to zero to mimic a 2D plane strain problem.

The results are shown in Figure (11). As can be seen, the 2D and constrained 3D formulations give quite similar results, validating the present 2D formulation.

References

Arruda, E.M., Boyce, M.C., 1993. A three-dimensional constitutive model for the large stretch behavior of rubber elastic materials. Journal of the Mechanics and Physics of Solids 41, 389–412.

Biddiss, E., Chau, T., 2008. Dielectric elastomers as actuators for upper limb prosthetics: challenges and opportunities. Medical Engineering and Physics 30, 403–418.

Brochu, P., Pei, Q., 2010. Advances in dielectric elastomers for actuators and artificial muscles. Macromolecular Rapid Communications 31, 10–36.

Buschel, A., Klinkel, S., Wagner, W., 2013. Dielectric elastomers - numerical modeling of nonlinear visco-electroelasticity. International Journal for Numerical Methods in Engineering 93, 834–856.

Carpi, F., Bauer, S., Rossi, D.D., 2010. Stretching dielectric elastomer performance. Science 330, 1759–1761.

Chen, D., Cai, S., Suo, Z., Hayward, R.C., 2012. Surface energy as a barrier to creasing of elastomer films: an elastic analogy to classical nucleation. Physical Review Letters 109, 038001.

Chiba, S., Waki, M., Kornbluh, R., Pelrine, R., 2008. Innovative power generators for energy harvesting using electroactive polymer artificial muscles. Proceedings of the SPIE 6927, 692715.

Dorfmann, A., Ogden, R.W., 2005. Nonlinear electroelasticity. Acta Mechanics 82, 99–127.

Dorfmann, A., Ogden, R.W., 2006. Nonlinear electroelastic deformations. Journal of Elasticity 174, 167–183.

Fox, J.W., Goulbourne, N.C., 2008. On the dynamic electromechanical loading of dielectric elastomer membranes. Journal of the Mechanics and Physics of Solids 56, 2669–2686.

Goulbourne, N.C., Mockensturm, E.M., Frecker, M.I., 2005. A nonlinear model for dielectric elastomer membranes. Journal of Applied Mechanics 72, 899–906.

Henann, D.L., Bertoldi, K., 2014. Modeling of elasto-capillary phenomena. Soft Matter 10, 709–717.

Henann, D.L., Chester, S.A., Bertoldi, K., 2013. Modeling of dielectric elastomers: design of actuators and energy harvesting devices. Journal of the Mechanics and Physics of Solids 61, 2047–2066.

Javili, A., Steinmann, P., 2010. A finite element framework for continua with boundary energies. part II: the three-dimensional case. Computer Methods in Applied Mechanics and Engineering 199, 755–765.

Keplinger, C., Kaltenbrunner, M., Arnold, N., Bauer, S., 2010. Rontgen's electrode-free elastomer actuators without electromechanical pull-in instability. Proceedings of the National Academy of Science 107, 4505–4510.

Keplinger, C., Li, T., Baumgartner, R., Suo, Z., Bauer, S., 2012. Harnessing snap-through instability in soft dielectrics to achieve giant voltage-triggered deformation. Soft Matter 8, 285–288.

Figure 11: Comparison of 2D and constrained 3D results for inhomogeneous deformation of a single finite element.

Khan, K.A., Wafai, H., Sayed, T.E., 2013. A variational constitutive framework for the nonlinear viscoelastic response of a dielectric elastomer. Computational Mechanics 52, 345–360.

Kofod, G., Sommer-Larsen, P., 2005. Silicone dielectric elastomer actuators: finite-elasticity model of actuation. Sensors and Actuators A 122, 273–283.

Kofod, G., Sommer-Larsen, P., Kornbluh, R., Pelrine, R., 2003. Actuation response of polyacrylate dielectric elastomers. Journal of Intelligent Material Systems and Structures 14, 787–793.

Li, W., Landis, C.M., 2012. Deformation and instabilities in dielectric elastomer composites. Smart Materials and Structures 21, 094006.

Liu, J.L., Feng, X.Q., 2012. On elastocapillarity: a review. Acta Mechanica Sinica 28, 928–940.

McMeeking, R.M., Landis, C.M., 2005. Electrostatic forces and stored energy for deformable dielectric materials. Journal of Applied Mechanics 72, 581–590.

Mirfakhrai, T., Madden, J.D.W., Baughman, R.H., 2007. Polymer artificial muscles. Materials Today 10, 30–38.

Mora, S., Abkarian, M., Tabuteau, H., Pomeau, Y., 2011. Surface instability of soft solids under strain. Soft Matter 7, 10612–10619.

Park, H.S., Nguyen, T.D., 2013. Viscoelastic effects on electromechanical instabilities in dielectric elastomers. Soft Matter 9, 1031–1042.

Park, H.S., Suo, Z., Zhou, J., Klein, P.A., 2012. A dynamic finite element method for inhomogeneous deformation and electromechanical instability of dielectric elastomer transducers. International Journal of Solids and Structures 49, 2187–2194.

Park, H.S., Wang, Q., Zhao, X., Klein, P.A., 2013. Electromechanical instability on dielectric polymer surface: modeling and experiment. Computer Methods in Applied Mechanics and Engineering 260, 40–49.

Patrick, L., Gabor, K., Silvain, M., 2007. Characterization of dielectric elastomer actuators based on a hyperelastic film model. Sensors and Actuators A 135, 748–757.

Pei, Q., Pelrine, R., Rosenthal, M., Stanford, S., Prahlad, H., Kornbluh, R., 2004. Recent progress on electroelastomer artificial muscles and their application for biomimetic robots. Proceedings of the SPIE 5385, 41–50.

Pelrine, R., Kornbluh, R., Pei, Q., Joseph, J., 2000. High-speed electrically actuated elastomers with strain greater than 100%. Science 287, 836–839.

Pelrine, R.E., Kornbluh, R.D., Joseph, J.P., 1998. Electrostriction of polymer dielectrics with compliant electrodes as a means of actuation. Sensors and Actuators A 64, 77–85.

Pineirua, M., Bico, J., Roman, B., 2010. Capillary origami controlled by an electric field. Soft Matter 6, 4491–4496.

Plante, J.S., Dubowsky, S., 2006. Large-scale failure modes of dielectric elastomer actuators. International Journal of Solids and Structures 43, 7727–7751.

Plante, J.S., Dubowsky, S., 2007a. On the performance mechanisms of dielectric elastomer actuators. Sensors and Actuators A 137, 96–109.

Plante, J.S., Dubowsky, S., 2007b. On the properties of dielectric elastomer actuators and their design implications. Smart Materials and Structures 16, S227–S236.

Roman, B., Bico, J., 2010. Elasto-capillarity: deforming an elastic structure with a liquid droplet. Journal of Physics: Condensed Matter 22, 493101.

Saksono, P.H., Peric, D., 2006a. On finite element mod-

elling of surface tension. variational formulation and applications - part I: quasistatic problems. Computational Mechanics 38, 265–281.

Saksono, P.H., Peric, D., 2006b. On finite element modelling of surface tension. variational formulation and applications - part II: dynamic problems. Computational Mechanics 38, 251–263.

Schlaak, H.F., Jungmann, M., Matysek, M., Lotz, P., 2005. Novel multilayer electrostatic solid-state actuators with elastic dielectric. Proceedings of the SPIE 5759, 121–133.

Simo, J.C., Taylor, R.L., Pister, K.S., 1985. Variational and projection methods for the volume constraint in finite deformation elasto-plasticity. Computer Methods in Applied Mechanics and Engineering 51, 177–208.

Suo, Z., 2010. Theory of dielectric elastomers. Acta Mechanica Solida Sinica 23, 549–578.

Suo, Z., Zhao, X., Greene, W.H., 2008. A nonlinear field theory of deformable dielectrics. Journal of the Mechanics and Physics of Solids 56, 467–486.

Tahoe, 2015. http://sourceforge.net/projects/tahoe/ .

Vu, D.K., Steinmann, P., Possart, G., 2007. Numerical modelling of non-linear electroelasticity. International Journal for Numerical Methods in Engineering 70, 685–704.

Wang, Q., Liu, C.T., Yang, Y., Dong, Y.D., Lu, J., 2011a. Atomic-scale structural evolution and stability of supercooled liquid of a zr-based bulk metallic glass. Physical Review Letters 106, 215505.

Wang, Q., Suo, Z., Zhao, X., 2012a. Bursting drops in solid dielectrics caused by high voltages. Nature Communications 3, 1157.

Wang, Q., Tahir, M., Zang, J., Zhao, X., 2012b. Dynamic electrostatic lithography: multiscale on-demand patterning on large-area substrates. Advanced Materials 24, 1947–1951.

Wang, Q., Zhang, L., Zhao, X., 2011b. Creasing to cratering instability in polymers under ultrahigh electric fields. Physical Review Letters 106, 118301.

Wang, Q., Zhao, X., 2013. Creasing-wrinkling transition in elastomer films under electric fields. Physical Review E 88, 042403.

Wissler, M., Mazza, E., 2005. Modeling and simulation of dielectric elastomer actuators. Smart Materials and Structures 14, 1396–1402.

Wissler, M., Mazza, E., 2007. Mechanical behavior of an acrylic elastomer used in dielectric elastomer actuators. Sensors and Actuators A 134, 494–504.

Zhang, X.Q., Wissler, M., Jaehne, B., Broennimann, R., Kovacs, G., 2004. Effects of crosslinking, prestrain and dielectric filler on the electromechanical response of a new silicone and comparison with acrylic elastomer. Proceedings of the SPIE 5385, 78–86.

Zhao, X., Suo, Z., 2007. Method to analyze electromechanical instability of dielectric elastomers. Applied Physics Letters 91, 061921.

Zhao, X., Wang, Q., 2014. Harnessing large deformation and instabilities of soft dielectrics: theory, experiment, and application. Applied Physics Reviews 1, 021304.

Zhou, J., Hong, W., Zhao, X., Zhang, Z., Suo, Z., 2008. Propagation of instability in dielectric elastomers. International Journal of Solids and Structures 45, 3739–3750.